International Journal of Thermal Sciences 48 (2009) 1765–1776

Contents lists available at ScienceDirect

International Journal of Thermal Sciences

journal homepage: www.elsevier.com/locate/ijts

A comparative study on the air-side performance of wavy fin-and-tube heat exchanger with punched delta winglets in staggered and in-line arrangements

Liting Tian, Yaling He*, Yubing Tao, Wenquan Tao

State Key Laboratory of Multiphase Flow in Power Engineering, School of Energy & Power Engineering, Xi'an Jiaotong University, Xi'an 710049, China

ARTICLE INFO

Article history:
Received 15 April 2008
Received in revised form
6 February 2009
Accepted 6 February 2009
Available online 17 March 2009

Keywords:
Longitudinal vortices
Delta winglet
Wavy fin-and-tube heat exchanger
In-line
Staggered

ABSTRACT

The air-side heat transfer and fluid flow characteristics of wavy fin-and-tube heat exchanger with delta winglets are investigated numerically. The three-dimensional simulations are performed with renormalization-group (RNG) $k-\varepsilon$ model to lay the foundation for the design of the high-performance heat exchanger. The wavy fin-and-tube heat exchangers which have three-row round tubes in staggered or in-line arrangements are studied. The numerical results show that each delta winglet generates a downstream main vortex and a corner vortex. For the in-line array, the longitudinal vortices enhance the heat transfer not only on the fin surface in the tube wake region but also on the tube surface downstream of the delta winglet; for the staggered array, longitudinal vortices are disrupted at the first wavy trough downstream from the delta winglet and only develop a short distance along the main-flow direction, and the vortices mainly enhance the heat transfer of the fin surface in the tube wake region. The longitudinal vortices generated by delta winglet cause considerable augmentation of heat transfer performance for wavy fin-and-tube heat exchanger with modest pressure drop penalty. When $Re_{D_c} = 3000$, compared with the wavy fin, the j and f factors of the wavy fin with delta winglets in staggered and in-line arrays are increased by 13.1%, 7.0% and 15.4%, 10.5%, respectively.

1. Introduction

Fin-and-tube heat exchangers are widely employed in many power engineering and chemical engineering applications, especially in heating, ventilation, air-conditioning, and refrigeration (HVACR) systems. Generally, a liquid flows through the tubes and a gas flows through the channels formed by the neighboring fins. Because the thermal resistance of gas is inherently higher than that of liquid, the dominant thermal resistance of fin-and-tube heat exchanger is usually on the gas side (generally air-side), which may account for 85% or more of the total thermal resistance. The use of enhanced fin surface is the most effective way to improve the overall performance of the fin-and-tube heat exchanger to meet the demand of high efficiency and low cost. Fins employed on the gas side can increase the heat exchanger surface area and strengthen the flow disturbance. Typically, these enhanced surfaces are developed from corrugated fin to interrupted fin (such as slits, louvers, and offset-strip fin). The wavy surface can periodically change the main-flow direction and cause better flow mixing, the slit or louvered-fin can periodically interrupt the main-flow, break and renew the thermal boundary layer.

Jacobi and Shah [1] indicated that heat transfer enhancement consists of main-flow enhancement and secondary flow enhancement. Louvered and slit fins and wavy fin are examples of main-flow enhancement method. The intentional generation of vortices to enhance heat transfer is a secondary flow enhancement method. The longitudinal vortex has already been successfully applied on the fin surface of the core for heat transfer enhancement. Longitudinal vortex generators (LVGs), as a special extended surface, are usually incorporated into a heat transfer surface with an attack angle by means of embossing, stamping, or punching process. When the fluid flows over the LVGs, the pressure difference across the vortex generator causes flow separation and induces vortices downstream.

The longitudinal vortices were first used in boundary layer control by Schubauer and Spangenberg [2] in 1960. Jonhnson and Joubert [3] first reported the impact of vortex generators on the heat transfer in 1969. Later, the use of LVGs in channel flow applications has received considerable attentions. Jacobi and Shah [1] provided an excellent review of heat transfer enhancement through the use of longitudinal vortices. Gentry and Jacobi [4,5] experimentally studied the heat transfer enhancement performance of delta wing vortex generators in a flat-plate flow by

* Corresponding author. Tel.: +86 29 8266 3300; fax: +86 29 8266 7745.
E-mail address: yalinghe@mail.xjtu.edu.cn (Y.L. He).

1290-0729/$ – see front matter © 2009 Elsevier Masson SAS. All rights reserved.
doi:10.1016/j.ijthermalsci.2009.02.007

Nomenclature

A	cross-sectional area, m^2
A_c	minimum flow cross-sectional area, m^2
A_f	fin surface area, m^2
A_0	total surface area, m^2
c_p	specific heat of the fluid, $J\,kg^{-1}\,K^{-1}$
D_c	tube outside diameter, m
D_h	$4A_cL/A_0$, hydraulic diameter, m
f	friction factor
F_p	fin pitch, m
h	heat transfer coefficient, $W\,m^{-2}\,K^{-1}$ or height of the delta winglet, m
H	channel height, m
j	Colburn factor
k	turbulence kinetic energy, $m^2\,s^{-2}$
l	length of the delta winglet, m
L	fin length along flow direction, m
Nu	Nusselt number
p	pressure, Pa
Δp	pressure drop in flow direction, Pa
P_l	longitudinal tube pitch, m
P_t	transverse tube pitch, m
Pr	Prandtl number
q	heat flux, $W\,m^{-2}$
Q	heat transfer rate, W
Re_{D_c}	Reynolds number based on tube outside diameter
T	temperature, K
u, v, w	x, y, z velocity components, $m\,s^{-1}$
u_m	mean velocity at the minimum flow cross-sectional area, $m\,s^{-1}$
$\vec{U}$	velocity vector, $m\,s^{-1}$
x, y, z	Cartesian coordinates
X	x/H
X_L	$\sqrt{(P_t/2)^2 + P_l^2}/2$, geometric parameter, m
X_M	$P_t/2$, geometric parameter, m

Greek symbols

α	circumferential angle, °
β	attack angle of the delta winglet, °
δ_f	fin thickness, m
μ	dynamic viscosity, $kg\,m^{-1}\,s^{-1}$
ρ	density, $kg\,m^{-3}$
λ	thermal conductivity, $W\,m^{-1}\,K^{-1}$
ε	turbulent energy dissipation rate, $m^2\,s^{-3}$
Γ	circulation of cross-section, $m^2\,s^{-1}$
θ	wavy angle of fin, °
Θ	dimensionless temperature
η_f	fin efficiency
η_0	surface efficiency

Subscripts

a	air
f	fin
in	inlet
m	mean
out	outlet
w	tube wall
x	local

a naphthalene sublimation technique. The results indicated that the average heat and mass transfer could be enhanced by 50–60% at low Reynolds number over the unenhanced performance. Biswas et al. [6] carried out numerical and experimental studies on flow structure and heat transfer performance of longitudinal vortices behind a delta winglet placed in a fully developed laminar channel flow. In recent years, LVGs are widely applied in various heat exchangers to increase the heat transfer coefficient with only small increase in pressure drop penalty, which have been studied by many researchers. Wang et al. [7] utilized a dye-injection technique to visualize the flow structure for enlarged plain fin-and-tube heat exchanger with annular and delta winglet vortex generators. They found that for the same winglet height, the delta winglet showed more intensive vertical motion and flow unsteadiness than annular winglet, however, the corresponding pressure drop of the delta winglet was lower than that of annular winglet. Chen et al. [8,9] explored the heat transfer enhancement and pressure drop increase of finned oval-tube heat exchanger with punched delta-winglet pairs in staggered and in-line arrangements. Tiwari et al. [10] made a numerical study on laminar flow and heat transfer in a channel with built-in oval-tube and delta winglets, the different attack angles and the axial locations of the winglets were considered. The results indicated that vortex generators in conjunction with the oval-tubes could definitely enhance the improvement of fin-tube heat exchangers. O'Brien et al. [11] presented an experimental study on forced convection heat transfer in a narrow rectangular duct fitted with an oval-tube and one or two delta-winglet pairs. Mean heat transfer results indicated that the oval-tube geometry with single winglet pair yielded significant heat transfer enhancement, the average heat transfer performance was about 38% higher than the oval-tube without winglet, and the corresponding increase in friction factor was limited to less than 10%. Then O'Brien et al. [12] made an experimental study in a narrow duct fitted with a circular tube and/or a delta-winglet pair. The results of overall mean fin surface Nusselt number indicated a significant heat transfer enhancement with the winglets and circular tube. At the lowest Reynolds number, the enhancement was nearly a factor of 2. At the higher Reynolds number, the enhancement was close to 50%. Leu et al. [13] carried out numerical and experimental analyses to study the effects of different attack angles ($\beta = 30°$, 45° and 60°) on enhanced heat transfer in a three-row plain fin-and-tube heat exchanger with rectangular winglets, they reported that the case of $\beta = 45°$ provided the best heat transfer enhancement. Pesteei et al. [14] experimentally studied the effect of winglet location on heat transfer enhancement and pressure drop in plain fin-and-tube heat transfer. Biswas et al. [15] presented a numerical investigation of the flow structure and heat transfer enhancement in a channel with a built-in circular tube and a pair of delta winglets. The results showed that the longitudinal vortices generated by the winglets placed in the wake region behind the tube enhanced the local heat transfer by 240%. Torii et al. [16] proposed a novel delta winglet configuration, called common-flow-up. The proposed configuration was shown to be effective in delaying boundary layer separation from the tube, reducing form drag, and removing the zone of poor heat transfer from the near-wake of the tube. Heat transfer enhancement and pressure drop caused by delta winglets were compared between common-flow-up and common-flow-down configurations by Kwak et al. [17]. Allison et al. [18] presented an experimental analysis of the effects of delta winglets on the performance of a fin-and-flat tube radiator, the winglets were arranged in common-flow-up configuration and placed directly upstream of the tube.

The results were compared with a standard louvered-fin surface, the winglet surface had 87% of the heat transfer capacity but only 53% of the pressure drop of the louvered-fin surface. Wang et al. [19] experimentally studied the local and average heat transfer characteristics of a complete flat tube-fin element with four vortex generators per tube in common-flow-down configuration, results revealed that LVGs could efficiently enhance the heat transfer in the region near flat tube on fin surface mounted with LVGs. Jocabi and his co-worker [20,21] did a lot of work on the LVGs, they applied wing-type LVGs in the offset-strip fin array and the flat tube louvered-fin compact heat exchanger. Sanders et al. [22] had combined the winglet and louvered-fin heat exchanger, the experimental studies presented the heat transfer augmentation along the tube wall through the use of winglets. Dupont et al. [23] made an experimental study of the flow in a model channel of plate–fin heat exchanger with periodically arranged smooth embossed-type vortex generators. The flow field showed the existence of strong longitudinal vortices behind each vortex generator, and these smooth shaped vortex generators were very promising for enhanced heat exchangers.

The foregoing literature reviews show that the LVGs can generate the secondary flow deliberately, swirl flow, make flow destabilized and interrupt the boundary layer in the flow field, which can efficiently enhance heat transfer. Nowadays, the LVGs have been applied in various fin-and-tube heat exchangers in order to improve the air-side heat transfer, such as the plain fin-and-tube heat exchanger with round, oval or flat tube, the offset-strip fin and the louvered-fin compact heat exchangers. However, there is no report about LVGs applied to wavy fin-and-tube heat exchangers. The wavy fin can increase the heat transfer area, periodically change the main-flow direction and cause better air flow mixing and is widely used in air-conditioning and refrigeration fields. Tao et al. [24,25] numerically studied the air-side heat transfer and fluid flow characteristics of wavy fin heat exchangers with circular and elliptic tubes by body fitted coordinates. The effects of some parameters, such as wavy angle, fin pitch and tube row number, on the heat transfer and fluid flow performances were examined. The simulation results of Tao et al. [26] showed that in the tube wake region the local Nusselt number was very low, which indicated that in this region, the convective heat transfer was weak. So we can improve the overall heat transfer performance of the wavy fin-and-tube heat exchanger by adopting some enhanced approaches in the wake region behind the tube.

The application of the delta winglet longitudinal vortex generators can effectively improve the heat transfer performance in the tube wake region. This has motivated the present investigation. In present investigation, a new fin pattern is proposed by punching delta winglets on the wavy fin surface. The heat transfer and fluid flow characteristics of the wavy fin-and-tube heat exchanger with delta winglets are numerically studied and the comparisons between staggered and in-line arrangements are performed. In order to lay the foundation for the design of the high-performance heat exchanger, the present study also focuses on the better understanding of the complex flow and heat transfer interactions that occur when implementing delta winglet vortex generators in a wavy fin-and-tube heat exchanger.

2. Model description

The schematic view of this new fin pattern in staggered and in-line arrangements is shown in Fig. 1. The schematic diagram of a wavy fin-and-tube heat exchanger with delta winglet longitudinal vortex generators is shown in Fig. 2, which has three-row round tubes in staggered or in-line arrangement. A pair of delta winglets is punched out from the wavy fin symmetrically behind each round tube. The position of delta winglets and the relevant geometric dimensions for this heat exchanger are also shown in Fig. 2. The tube outside diameter D_c is 10.55 mm, longitudinal tube pitch P_l is 21.65 mm, transverse tube pitch P_t is 25 mm, fin pitch F_p is 3.2 mm, fin thickness δ_f is 0.2 mm, wavy angle of the fin θ is 15°. The base length l and height h of delta winglet are 5 mm and 2.5 mm, respectively. Since the delta winglet is punched from the wavy fin, the width of the delta winglet is equal to the fin thickness. The attack angle of the delta winglet β is 30°. In this study, we define that x, y, z are streamwise, normal, and spanwise coordinates, respectively, and y stands for the fin pitch direction. Due to symmetry, the region sketched by the dashed lines in Fig. 2 is selected as the computational domain, and the neighboring two fins' centric surfaces are selected as the upper and lower boundaries of the computational domain. Due to the relatively high heat transfer coefficient on the inner wall of the tube and the high thermal conductivity of the tube wall, the tube is assumed to be constant temperature. However, the temperature distribution in the fin surface has to be determined by solving the conjugate problem, in which both the temperature distribution in the solid fin surface and in the fluid need to be determined simultaneously [27]. Due to the fin thickness, the air velocity profile is not uniform at the entrance of the channel formed by the fins' centric surfaces. The computational domain is then extended upstream 10 times of the fin spacing so that a uniform velocity distribution can be ensured at the domain inlet. The computational domain is also extended downstream 30 times of the fin spacing in order to avoid the recirculation at the computational domain outlet, and hence the outflow boundary condition can be applied. To save the space, the extended domain is not presented in scale with the fin length in Fig. 2.

3. Mathematical formulation and numerical method

3.1. Governing equations and boundary conditions

Due to the small air temperature difference over the fin length, the air is considered as an incompressible fluid with constant physical properties. The flow in the computational domain is assumed to be three-dimensional, turbulent, steady and no viscous dissipation. The governing equations including continuity, momentum (Reynolds-averaged Navier–Stokes (RANS) equations) and energy equation for the fluid domain can be expressed as follows.

Continuity equation:

$$\frac{\partial}{\partial x_i}(\rho u_i) = 0 \tag{1}$$

Momentum equation:

$$\frac{\partial}{\partial x_i}(\rho u_i u_j) = -\frac{\partial p}{\partial x_j} + \frac{\partial}{\partial x_i}\left[\mu\left(\frac{\partial u_i}{\partial x_j} + \frac{\partial u_j}{\partial x_i} - \frac{2}{3}\delta_{ij}\frac{\partial u_k}{\partial x_k}\right)\right] + \frac{\partial}{\partial x_i}\left(-\rho\overline{u_i' u_j'}\right) \tag{2}$$

where,

$$-\rho\overline{u_i' u_j'} = \mu_t\left(\frac{\partial u_i}{\partial x_j} + \frac{\partial u_j}{\partial x_i}\right) - \frac{2}{3}\left(\rho k + \mu_t\frac{\partial u_k}{\partial x_k}\right)\delta_{ij} \tag{3}$$

The effect of turbulence on the flow field is included through the application of RNG $k-\varepsilon$ turbulence model [28]. The turbulence kinetic energy, k, and its dissipation rate, ε, are obtained from the following transport equations:

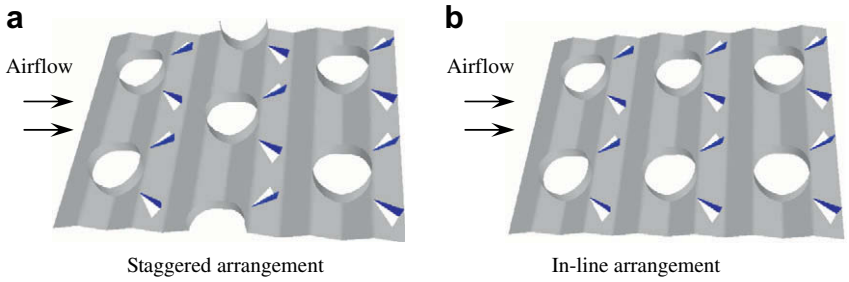

Fig. 1. Schematic view of a wavy fin with delta winglets.

Kinetic energy,

$$\frac{\partial}{\partial x_i}(\rho k u_i) = \frac{\partial}{\partial x_i}\left(\alpha_k \mu_{\text{eff}} \frac{\partial k}{\partial x_i}\right) + \mu_t S^2 - \rho\varepsilon \tag{4}$$

Dissipation rate,

$$\frac{\partial}{\partial x_i}(\rho \varepsilon u_i) = \frac{\partial}{\partial x_i}\left(\alpha_\varepsilon \mu_{eff} \frac{\partial \varepsilon}{\partial x_i}\right) + C_{1\varepsilon}\frac{\varepsilon}{k}\mu_t S^2 - C_{2\varepsilon}\rho\frac{\varepsilon^2}{k} - R_\varepsilon \tag{5}$$

where, $\mu_{\text{eff}} = \mu + \mu_t$ and $\mu_t = \rho C_\mu k^2/\varepsilon$ in the high Reynolds number range with $C_\mu = 0.0845$. S is the modulus of the mean rate of strain tensor, defined as $S = (2S_{ij}S_{ij})^{1/2}$, $S_{ij} = 1/2(\partial u_j/\partial x_i + \partial u_i/\partial x_j)$. The quantities α_k and α_ε are the inverse effective Prandtl numbers for k and ε, respectively.

The rate of strain term R_ε is given by

$$R_\varepsilon = \frac{C_\mu \rho \eta^3 (1 - \eta/\eta_0)}{1 + \beta\eta^3}\frac{\varepsilon^2}{k} \tag{6}$$

where, $\eta \equiv Sk/\varepsilon$, $\eta_0 = 4.38$, $\beta = 0.012$. The RNG $k-\varepsilon$ turbulence model constants have the following default values: $C_{1\varepsilon}$=1.42, $C_{2\varepsilon}$=1.68.

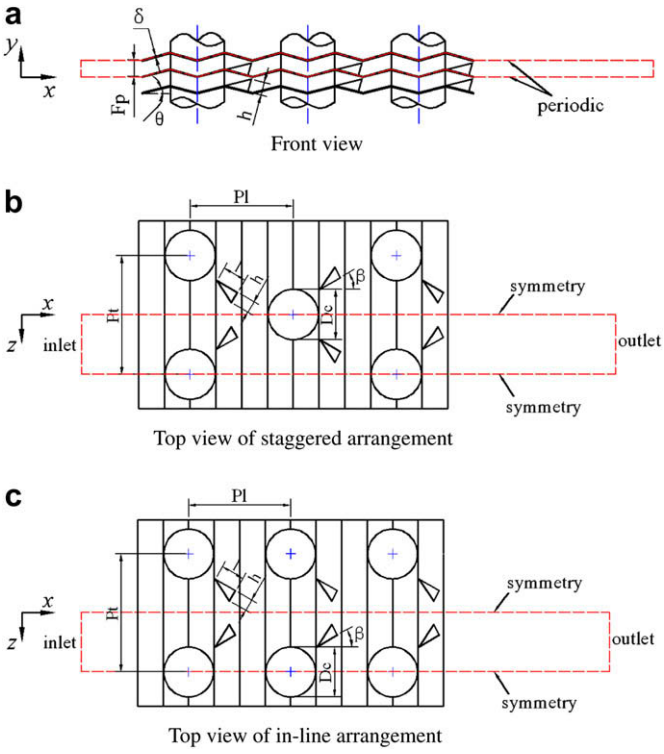

Fig. 2. Physical model and relevant geometrical parameters of the wavy fin-and-tube heat exchanger with delta winglets.

Energy equation:

$$\frac{\partial}{\partial x_i}[u_i(\rho E + p)] = \frac{\partial}{\partial x_i}\left(k_{\text{eff}}\frac{\partial T}{\partial x_i}\right) \tag{7}$$

where E is the total energy, k_{eff} is the effective thermal conductivity ($k + k_t$, where k_t is the turbulent thermal conductivity, defined according to the turbulent model being used).

For this model, fluid–solid conjugate heat transfer is taken into account and the solid is assumed isotropic, thermal contact resistance between the tube and the collar is ignored, and the energy equation solved in solid domain (fins and delta winglets) is given by

$$\frac{\partial}{\partial x_i}\left(\lambda_f \frac{\partial T}{\partial x_i}\right) = 0 \tag{8}$$

because the governing equations are elliptic in spatial coordinates, the boundary conditions are required for all boundaries of the computational domain. The temperature of the tube wall is higher than that of the inlet air. The required boundary conditions are described for the three regions as follows.

(1) In the upstream extended region (domain inlet)

At the inlet boundary: the air is assumed to have uniform velocity u_{in}, temperature T_{in}, the velocity components in the y and z directions are considered to be zero, the turbulent intensity is defined as the correlation suggested in the Fluent User's Manual [28] $I = 0.16\, Re_{D_h}^{-1/8}$.

At the upper and lower boundaries: periodic boundary conditions.

At the front and back boundaries: symmetric boundary conditions.

(2) In the downstream extended region (domain outlet)

At the upper and lower boundaries: periodic boundary conditions.

At the front and back boundaries: symmetric boundary conditions.

At the outlet boundary: streamwise gradient for all the variables are set to zero.

(3) In the fin coil region.

At the upper and lower boundaries: at the fin surface, no-slip conditions and adiabatic conditions are defined; at the punched holes under the delta winglets, periodic boundary conditions are assigned.

At the front and back boundaries:

Fluid region: symmetric boundary conditions.

Fin surface region: no-slip conditions and adiabatic conditions are defined.

Tube surface region: no-slip conditions and constant temperature T_w are defined.

Additionally, on the delta winglet surfaces, no-slip conditions for the velocity are specified, heat convection to the delta winglets and heat conduction in the delta winglets are considered simultaneously.

3.2. Numerical methods

The foregoing governing equations and the boundary conditions are solved by a commercial computational fluid dynamics code (FLUENT 6.2). A preprocessor GAMBIT 2.2.3 is used to create the model drawing and the required mesh for the solver. The multi-block hybrid approach is used to generate the mesh for the numerical simulation. The computational domain is divided into several subdomains, the subdomains localized around the delta winglets are meshed with tetrahedral elements, the subdomains localized around the tubes are meshed with hexahedral/wedge elements, the extended domains are meshed with hexahedral elements. For application of the periodic boundary condition, the meshes are matched by linking the periodic surfaces. In general, the computational domain is discretized with the fine grids in the fin coil region to resolve the swirling flow and the coarse grids in the extended regions to save the computing resource. The grids around the delta winglets and the tubes are shown in Fig. 3.

The governing equations are discretized by the finite volume method. The SIMPLE algorithm [27] is utilized to deal with the coupling of pressure and velocity. This numerical approach stores discrete values of the scalar variables at the center of the control volume. The face values of scalar variables are also required and their values are interpolated form the center values. The complex flow in the fin channel is not aligned with the grid. In order to obtain more accurate results, the second-order upwind scheme [27] is employed for the discretization of the convection terms, whereas the diffusion terms are discretized by the central difference scheme. The aforesaid governing equations are solved by a segregated implicit iterative scheme. To control the update of the computed variables at each iteration, the under-relaxation factors are varied between 0.3 and 1.0. The convergence criteria are that the residuals of the continuity, components of velocity, turbulent kinetic energy and dissipation rate are below 10^{-6}, and the residual of the energy is below 10^{-8}.

3.3. Parameter definition

To improve the physical understanding, some characteristic and non-dimensional parameters are defined as follows:

$$Re_{D_c} = \frac{\rho u_m D_c}{\mu} \tag{9}$$

$$Nu = \frac{hD_c}{\lambda} \tag{10}$$

where D_c is the tube outside diameter, u_m is the mean velocity at the minimum flow cross-sectional area A_c.

The heat transfer coefficient h is defined in terms of the heat transfer rate Q and the log-mean temperature difference, the heat transfer rate Q is determined by the aid of FLUENT.

$$h = \frac{Q}{\eta_0 A_0 \Delta T} \tag{11}$$

The log-mean temperature difference is expressed as:

$$\Delta T = \frac{(T_w - T_{in}) - (T_w - T_{out})}{\ln[(T_w - T_{in})/(T_w - T_{out})]} \tag{12}$$

The surface efficiency η_0 in Eq. (11) is calculated from the fin efficiency η_f.

$$\eta_0 = 1 - \frac{A_f}{A_0}\left(1 - \eta_f\right) \tag{13}$$

where A_f is the fin surface area, A_0 is the total surface area.

η_f is obtained by using Schmidt's method [29].

$$\eta_f = \frac{\tanh(mr\phi)}{mr\phi} \tag{14}$$

where $r = 0.5D_c$, $m = \sqrt{2h/(\lambda_f \delta_f)}$, $\phi = (R_{eq}/r - 1)[1 + 0.35 \ln(R_{eq}/r)]$, $R_{eq}/r = 1.27 X_M/r(X_L/X_M - 0.3)^{0.5}$, $X_L = \sqrt{(P_t/2)^2 + P_l^2}/2$ and $X_M = P_t/2$, λ_f is fin thermal conductivity.

The span-averaged local heat transfer coefficient h_x is defined by:

$$h_x = \frac{q_x}{T_{f,x} - T_{a,x}} \tag{15}$$

where q_x is the span-averaged local heat flux, $T_{f,x}$ is the span-averaged local wall temperature, $T_{a,x}$ is the mass-weighted average air temperature of the cross-section.

The circulation of the cross-section is defined by:

$$\Gamma_x = \int \xi dA = \int |\nabla \times \vec{U}| dA \tag{16}$$

The Colbum factor j is used to describe the heat transfer performance.

$$j = \frac{Nu}{RePr^{1/3}} = \frac{h}{\rho u_m c_p} Pr^{2/3} \tag{17}$$

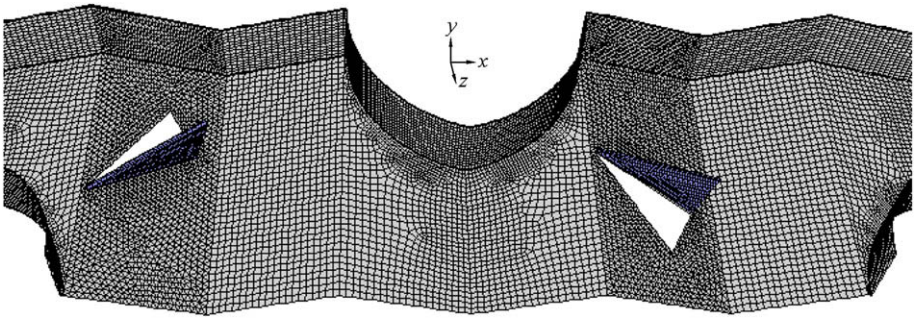

Fig. 3. Grid system around delta winglets and tubes.

The friction factor f is used to describe the pressure loss characteristics.

$$f = \frac{\Delta p}{\frac{1}{2}\rho u_m^2} \cdot \frac{A_c}{A_0} \tag{18}$$

4. Validation of the model and grid independence

4.1. Grid independence

Grid independence is necessarily investigated to ensure the accuracy and validity of the numerical results. The grid independent study is performed on the wavy fin-and-tube heat exchanger with delta winglets in staggered array for $Re_{D_c} = 3000$. In order to investigate the influence of the grid density on the computational results, three sets of grid number are studied, they are about 121,000, 196,000, 384,000 cells. The results of the three sets of grid number are tabulated in Table 1, the relative errors of the Nusselt number and the friction factor between the grid 384,000 and grid 196,000 are less than 1% and 2%, respectively. Thus to save computer resource and keep a balance between computational economics and accuracy, the adopted grid number in the computational domain is about 196,000.

4.2. Model verification

In order to validate the reliability of the computational model and numerical method, numerical simulation is carried out at the same fin geometrical configurations and operating conditions as presented in [30], the computation is conducted for the three-row wavy fin-and-tube heat exchanger in staggered array. The Reynolds number Re_{D_c} ranges from 500 to 5000, the corresponding frontal air velocity ranges from 0.4 m s^{-1} to 4.0 m s^{-1}. Prior to conducting the numerical computations, a question may be raised as whether the steady state computational model is suitable. Recently, Xue and Min [31] performed a comparative study for flow in corrugated channels by using steady and transient models with the same conditions. They found that when the flow reached periodic unsteady regime, it was appropriate to use steady model to predict the averaged Nusselt number and friction factor. He et al. [32] conducted a comparison between steady and unsteady models for plain fin-and-tube heat exchanger at $Re = 5000$ based on tube outside diameter. It was found that the difference in the averaged Nusselt number between these two models was only about 0.35%. From the engineering point of view, the most important information is the averaged friction factor and the Nusselt number of the heat exchangers, so the steady model is adopted in present simulation.

The experimental observations and data for the flow regime transition in such complicated fin channel are not so well-accumulated and definite, as the ones for the flow in a simple channel. In the numerical simulation of plain fin-and-tube heat exchanger with winglet type vortex generators, some researchers like Biswas et al. [15] use unsteady laminar model, other like Leu et al. [13] use steady turbulence model. For the wavy fin-and-tube heat exchanger with delta winglets, due to the wavy fins and delta winglets, the transition to turbulence occurs at lower Reynolds numbers than plain fin-and-tube heat exchanger. In the present study, three different models, namely laminar model, standard $k-\varepsilon$ model and RNG $k-\varepsilon$ model, are chosen to simulate the flow in the fin channel. The RNG model has shown substantial improvements over the standard model where the flow feature includes strong streamline curvature, vortices, and rotation. The comparisons of the numerical and experimental results are provided in Fig. 4, where the experimental correlations of Nu and Δp are adopted from Ref. [30]. The RNG $k-\varepsilon$ model gives the best results, it satisfactorily predicts the relation of j/f and Re. The maximum deviation in Nu, Δp and j/f of RNG $k-\varepsilon$ model from experimental results are less than 10%, 11% and 3%, respectively, which are in good agreement with the experimental results, therefore, the RNG $k-\varepsilon$ model is selected in the present study. In addition, the model validation is performed through a comparison with the numerical results of Biswas et al. [15], the computation is conducted for a flat-plate channel with a built-in circular tube and a pair of delta winglets, the steady RNG $k-\varepsilon$ model is adopted in present simulation. The span-averaged Nusselt number distribution along the streamwise direction of the channel is compared in Fig. 5. It can be seen that the present computed results of the span-averaged Nusselt number agree well with the Biswas et al.'s results [15], with the mean deviation being 4% and the maximum deviation being 10%.

Table 1
Results of different gird numbers.

Grid number	121,000	196,000	384,000
Nu	40.96	42.41	42.82
f	0.0608	0.0579	0.0568

5. Numerical results and discussions

5.1. Longitudinal vortices generated by the delta winglet

Fig. 6(a) presents the streamlines starting from the first row tube and delta winglets in the wavy fin channel with in-line tube array for $Re_{D_c} = 3000$. The delta winglets are punched out from the wavy fin behind each tube, when the air flows over the delta winglet, the pressure difference between the front surface (facing the flow) and the back surface generates the longitudinal vortices. These vortices which rotating axes parallel to the main-flow direction develop downstream in company with the main-flow. At the same time, the strength of these longitudinal vortices decreases downstream due to the viscous dissipation. Fig. 6(b) presents the secondary velocity vectors of the cross-section ($x = 21$ mm) behind the trailing edge of the first row delta winglet. It can be seen that there are two vortices at the back of each delta winglet: a main vortex and a corner vortex. The intensity of the corner vortex is weaker than that of the main vortex. The left main vortex rotates in a clockwise direction, while the right main vortex rotates in a counterclockwise direction. The main vortex, located directly downstream of the delta winglet, is formed by flow separation at the leading edge of the delta winglet. The stronger main vortex causes secondary flow which induces the swirling motion and enhances the fluid transport from the mainstream region to the wake region behind the tube, and the size of the recirculating wake region behind the tube is reduced (as seen in Fig. 6(a)). Méndez et al. [33] have explained the kinematics of flow and the mechanism of transport enhancement due to longitudinal vortices. The corner vortex, located outside of the main vortex, has an opposite rotational direction to the main vortex. The corner vortex having a horseshoe vortex-like characteristic feature is generated at the junction of the upstream-facing pressure side of the winglet and the fin wall, wraps around the delta winglet and develops downstream together with the main-flow.

5.2. Comparison of the fluid flow characteristics

The fin channel configuration is changed with different arrangements of the tube bank, so the flow structure in it is also changed. Fig. 7 shows the variation of average pressure along the air

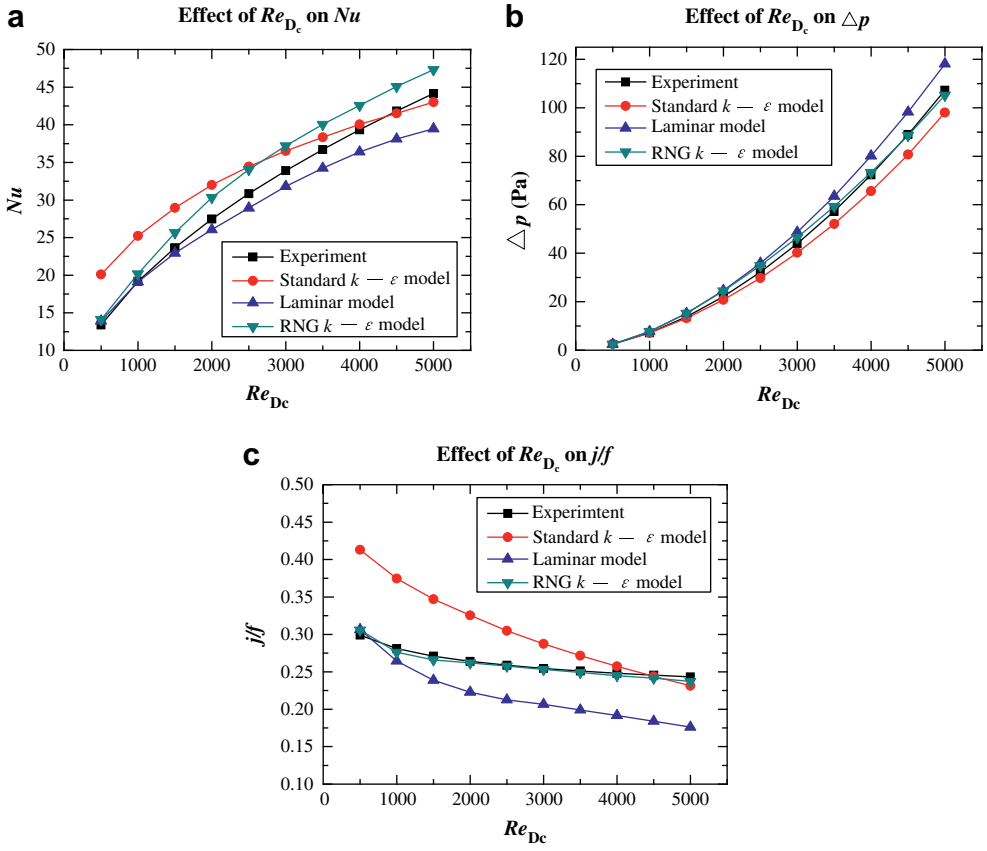

Fig. 4. Validation of numerical models with experimental results.

flow direction for the wavy fin with delta winglets in staggered and in-line arrays for $Re_{D_c} = 3000$. At the same time, the variations of average pressure for the wavy fin in staggered and in-line arrays without delta winglets are also shown for the comparison. The shadow region in the figure represents the axial location of the round tube. The average pressure at any cross-section is determined through the area-weighted average static pressure at this cross-section. The average pressure has a steep drop around the tube because of the drag effect formed by the tube, while the average pressure has a slight drop at the axial location corresponding to the delta winglet. Because the delta winglet shape is slender and the projected area of the delta winglet is very small, the form drag and the friction resistance contributed by the delta winglet are lower compared with the form drag of the round tube and the friction resistance of the wavy fin surfaces. As can be seen from the figure, the increase of the pressure drop penalty induced by the delta winglet is relatively small. In addition, the pressure drop of the staggered arrangement is larger than that of the in-line arrangement for the wavy fin with and without delta winglets.

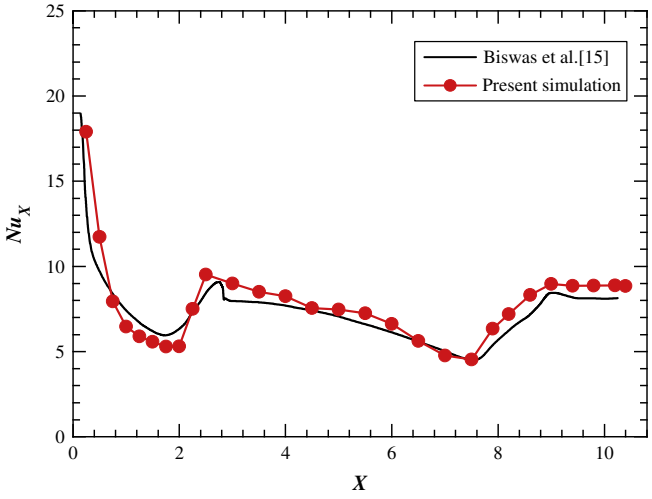

Fig. 5. Comparison of span-averaged Nusselt number between the computed results and reference's predictions.

The different arrangements of the tube bank can affect the development of the longitudinal vortices. Fig. 8 shows the circulation of the cross-section along the streamwise direction in staggered and in-line arrangements for $Re_{D_c} = 3000$. It can be seen that the circulation of the cross-section shows periodicity in the streamwise direction due to the periodic change of the flow cross-sectional area. As the flow encounters the tubes, the flow cross-sectional area gradually decreases and the flow accelerates, the vortices undergo compression and the circulation decreases until the axial location corresponding to the minimum flow cross-sectional area. On the back half of the tube, the flow gradually decelerates and the circulation gradually increases. For the staggered arrangement, when the incoming flow approaches each tube, the fluid reaches the front stagnation point and wraps around the tube to flow downstream, the horseshoe vortices are formed at the junction of the tube and the fin surface. The circulation has a peak value at the front stagnation point of the second and third row tubes, whereas, for the in-line arrangement, the front stagnation point of the second and third row tubes is in the wake region of the upstream tube, there is no local maximum of the circulation at the

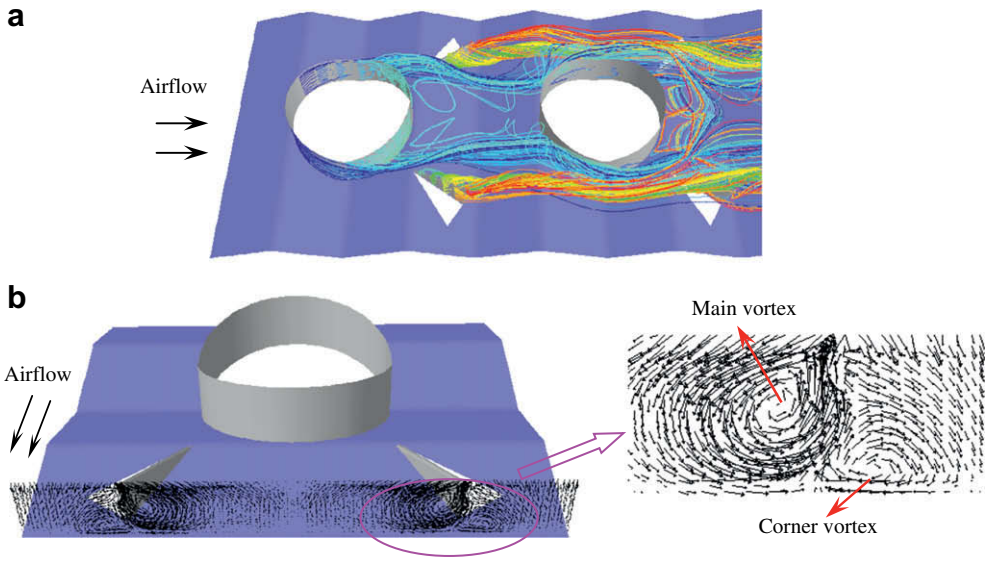

Fig. 6. (a) Streamlines starting from the first row tube and delta winglets. (b) Secondary velocity vectors at the cross-section of $x = 21$ mm downstream of the first row delta winglet in wavy fin channel with in-line tube array.

front portion of the second and third row tubes. For the wavy fin with delta winglets, in the in-line array, the circulation has an abrupt rise around the delta winglet and the increase trend persists for a long distance downstream of the delta winglet, the circulation of the wavy fin with delta winglets is always higher than that of the wavy fin without delta winglets until the position corresponding to the center of the downstream tube. In the staggered array, the circulation also has an abrupt rise around the delta winglet, but has a steep drop when the flow encounters the first wavy trough behind the delta winglet. This is because the main-flow direction changes at the downstream wavy trough and the downstream tube blocks the flow, the vortices are disrupted at the downstream wavy trough, and only develop a short distance in the streamwise direction.

For the wavy fin-and-tube heat exchanger with delta winglets, there are many geometrical factors which can affect the fluid flow characteristics. The tube layout, the delta winglets and the wavy fin together make the air flow complex in the channel between the two neighboring fins. Fig. 9 shows the velocity profiles in the middle plane of the fin channel, which is parallel to the fin surfaces, under the condition of $Re_{D_c} = 3000$. For the in-line array, the flow separates at the rear portion of a tube and reattaches at the front portion of the next tube, there are a large dead flow zones between the two adjacent tubes, which result in a large region of lower heat transfer between the tubes. When the fluid flows over the delta winglets punched on the fin behind the tubes (shown in Fig. 9(b)), the longitudinal vortices generated by the delta winglet increase the disturbance and mixing effects of the downstream air, and spur the main-flow to mix with the fluid in the tube wake. The separation from the main-flow is delayed and the wake region size is reduced. It can be seen that the area of the wake region in the wavy fin with delta winglets is obviously decreased and the area of the fin covered by the recirculating flow is also obviously compressed. For the wavy fin with delta winglets in the staggered array (shown in Fig. 9(d)), although the decrease of the wake region area behind the tube is not obvious compared with the in-line array, the velocity of the wake flow is increased.

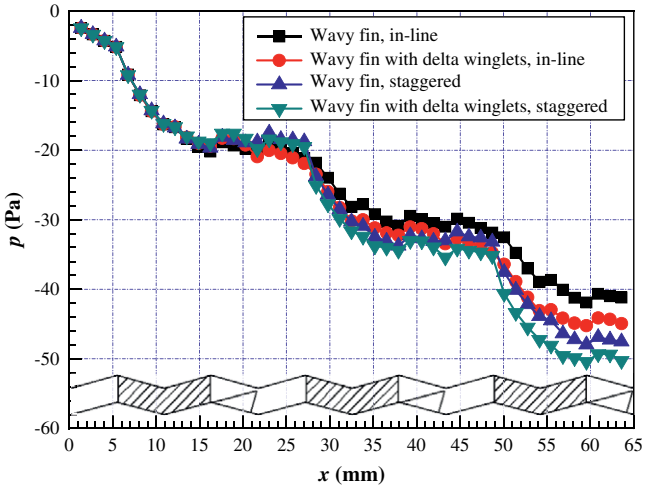

Fig. 7. Distribution of average pressure along streamwise direction in staggered and in-line arrangements.

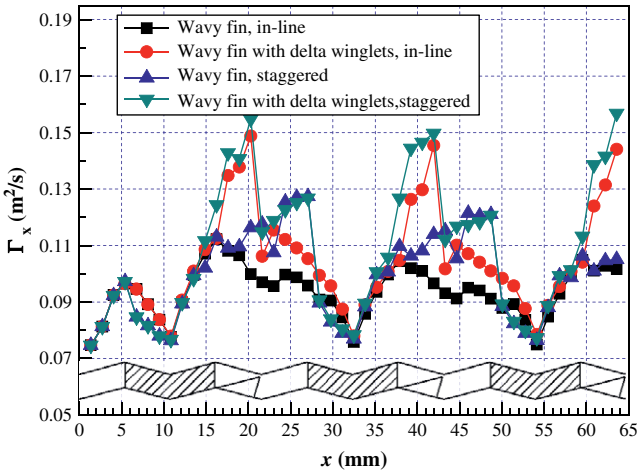

Fig. 8. Distribution of circulation of cross-section along streamwise direction in staggered and in-line arrangements.

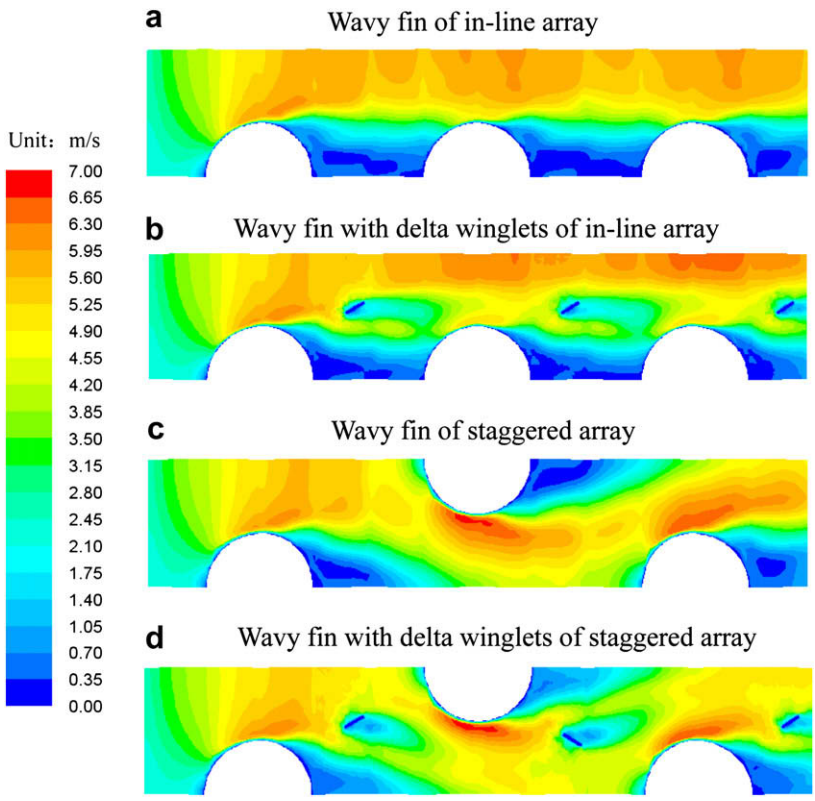

Fig. 9. Velocity profile in the middle plane of the fin channel in *y* direction for staggered and in-line arrays.

5.3. Comparison of the heat transfer characteristics

Fig. 10 shows the dimensionless temperature distributions $((T - T_{in})/(T_w - T_{in}))$ in the middle plane of the fin channel for the staggered and in-line arrays at $Re_{D_c} = 3000$. For the wavy fin with delta winglets, due to the generation of longitudinal vortices, the mixing between the main-flow with lower temperature and higher velocity and the wake flow with higher temperature and lower velocity is strengthened. So the wake region is compressed and the heat transfer coefficient of the fin surface in wake zone is enhanced, which means that the more heat quantity is transferred from the fins to the fluid. Fig. 10 presents that in both staggered and in-line arrays, the longitudinal vortices generated by the delta winglet decrease the wake region size behind the tube, and lead to the decrease of fluid temperature in the wake region. Compared with the wavy fin without delta winglets, the mixing of heat and cold fluid is more sufficient in the fin channel with delta winglets, and the temperature distribution in the outlet is more uniform. The temperature difference between the inlet and outlet of the fin channel with delta winglets increases, which indicates that the total heat transfer rate is increased. To sum up, in both staggered and in-line arrays, adding delta winglets on the wavy fin surface can obviously enhance the heat transfer of the wavy fin-and-tube heat exchanger.

In order to examine the heat transfer behavior along the flow direction, the span-averaged local heat transfer coefficient distribution along the streamwise direction in staggered and in-line arrangements for $Re_{D_c} = 3000$ is calculated and presented in Fig. 11. At the leading edge of the fin, the cool air comes into the fin channel for the first time, a thermal boundary layer on the fin wall gradually develops, the local heat transfer coefficient has a very high value and then decreases rapidly. For the in-line array (shown in Fig. 11(a)), the local heat transfer coefficient of the fin surface between the two adjacent tubes is lower due to the existence of the large wake region. While for the wavy fin with delta winglets, the longitudinal vortices modify the thermal boundary layer in the wake region and enhance the heat transfer between the two adjacent tubes, the local heat transfer coefficient has a peak value between the tubes. At the axial location of the delta winglet, a maximum increase of local heat transfer coefficient is up to 95% compared with the wavy fin without delta winglets. For staggered array (shown in Fig. 11(b)), an abrupt increase in local heat transfer coefficient is observed at the front stagnation point of each tube due to the formation of the horseshoe vortex system. In the wake region behind the tube, the convective heat transfer is very weak, there is a potential opportunity that the total heat transfer rate of wavy fin-and-tube heat exchanger can be improved by enhancing the local heat transfer coefficient of this wake region. For the wavy fin with delta winglets, at the axial location corresponding to the delta winglet, the local heat transfer coefficient also reaches a peak value due to the generation of longitudinal vortices, a maximum increase of local heat transfer coefficient is up to 80% compared with the wavy fin without delta winglets. In a word, in both staggered and in-line arrays, the longitudinal vortices generated by the delta winglet enhance the heat transfer of the fin surface in the wake region where the heat transfer is the weakest in the wavy fin-and-tube heat exchanger.

In order to study the effect of the longitudinal vortices generated by the delta winglet on the heat transfer of the tube surface, Fig. 12 presents the variation of span-averaged tube surface heat flux along the tube circumference from the first to the third row tube for both staggered and in-line arrays at $Re_{D_c} = 3000$. The angle α is measured from the front stagnation point of the tube. It can be seen that the variation trend of span-averaged heat flux along circumferential angle of the first row tube is greatly different from the second and third row tube for the in-line array, as shown

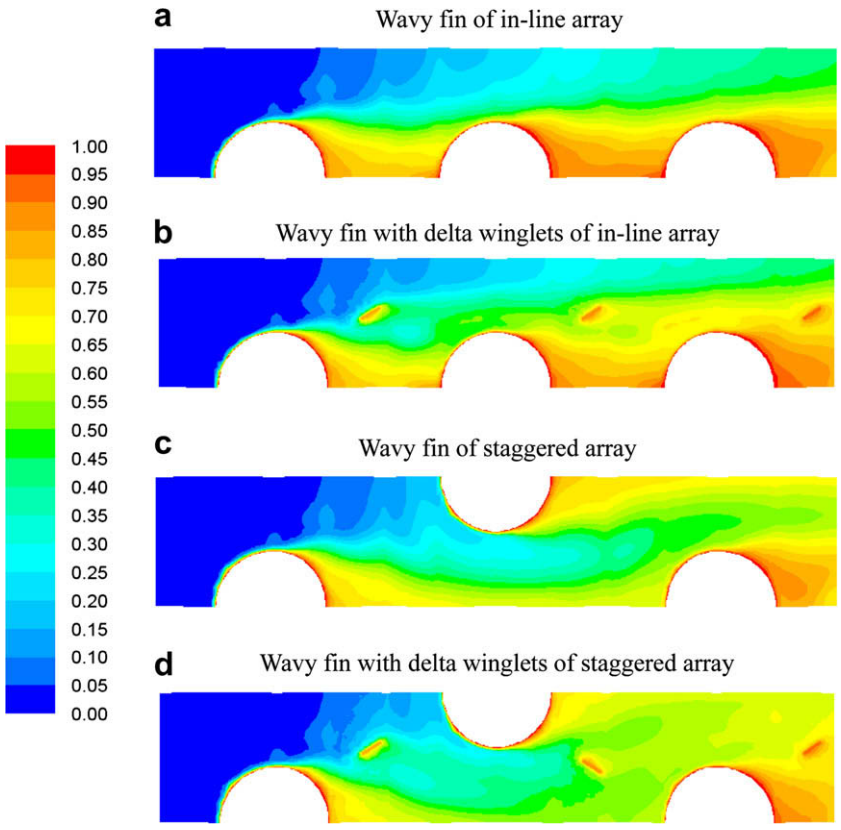

Fig. 10. Dimensionless temperature distribution in the middle plane of the fin channel in y direction for staggered and in-line arrays.

in Fig. 12(a). For the first row tube, the local heat flux is high at the front stagnation point and the front half of the tube, which has a maximum value at about $\alpha = 30°$. When the circumferential angle is larger than 100°, the flow separation occurs at the rear portion of the tube and the wake zone is formed behind the tube, the tube surface is covered by the wake flow, the local heat flux is quickly decreased. However, for the second and third row tubes, the front half of the tube is in the wake region of the upstream tube, the local heat flux at the front portion of the tube is very low, and gradually increases with the increase of the circumferential angle. The maximum value occurs at about $\alpha = 60°$, and later the local heat flux decreases with the increase of the circumferential angle. Like the first row tube, when the circumferential angle is larger than 100°, the tube surface is covered by the wake flow, and the local heat flux is also quickly decreased. It is interesting to note that the influence of the longitudinal vortices on the heat flux of the first row tube is very small, while, the effect of the delta winglets on the heat flux of the second and third row tube is more significant. In the in-line array, the longitudinal vortices generated by the delta winglet not only enhance the heat transfer of the fin surface in the wake region behind the tube, but also enhance the heat transfer of the tube surface downstream of the delta winglet. In the staggered array (shown in Fig. 12(b)), the change trend of the local heat transfer along the circumferential angle for each row tube looks similar, the value decreases in order from the first tube to the third tube. The local heat flux has a maximum value at the front stagnation point of the tube, and gradually decreases with the increasing of the circumferential angle. As the circumferential angle is larger than 100°, the tube surface is covered by the wake flow, the local heat flux is also quickly decreased. The longitudinal vortices

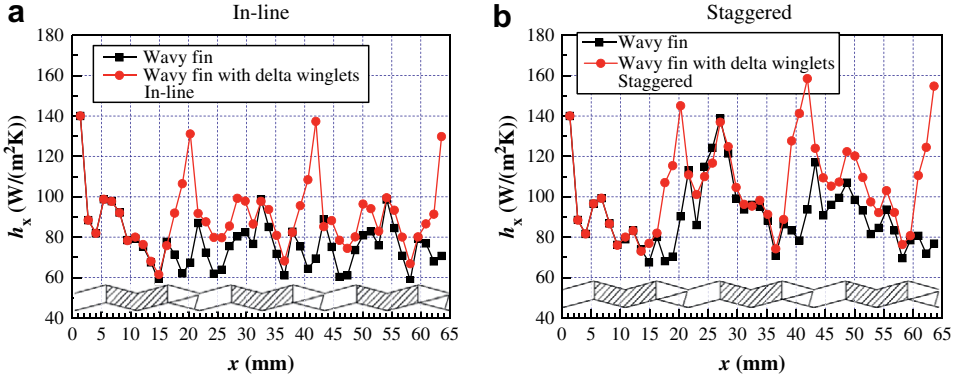

Fig. 11. Distribution of span-averaged heat transfer coefficient along streamwise direction in staggered and in-line arrangements.

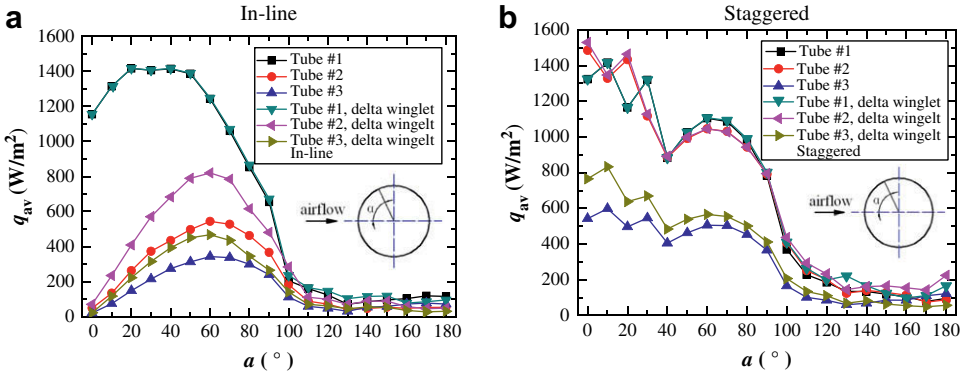

Fig. 12. Distribution of span-averaged tube surface heat flux along tube circumference in staggered and in-line arrangements.

have few effect on the local heat flux of the first and second row tube surface, for the third row tube, the heat flux enhancement is obvious.

In order to compare the heat transfer enhancement of the different row tubes by the longitudinal vortices, Fig. 13 shows the variation of the area-averaged tube surface heat flux for staggered and in-line arrangements. In the staggered array, compared with the wavy fin, the area-averaged tube surface heat flux of the first, second and third row tube in the wavy fin with delta winglets is increased by 3%, 4% and 18%, respectively. In the in-line array, compared with the wavy fin, the area-averaged tube surface heat flux of the first, second and third row tubes in the wavy fin with delta winglets is increased by 1%, 48% and 25%, respectively.

5.4. The overall performance

The Colbum and friction factors for the wavy fin with and without delta winglets in staggered and in-line arrangements at $Re_{D_c} = 3000$ are summarized in Table 2. It can be seen that in the staggered and in-line arrays, the delta winglet enhances the heat transfer of the wavy fin channel, and increases the pressure drop, but the increase of the heat transfer is larger than that of the pressure drop. In the in-line array, compared with the wavy fin, the j and f factors of the wavy fin with delta winglets are increased by 15.4% and 10.5%, respectively. In the staggered array, compared with the wavy fin, the j and f factors of the wavy fin with delta winglets are increased by 13.1% and 7.0%, respectively. Heat transfer

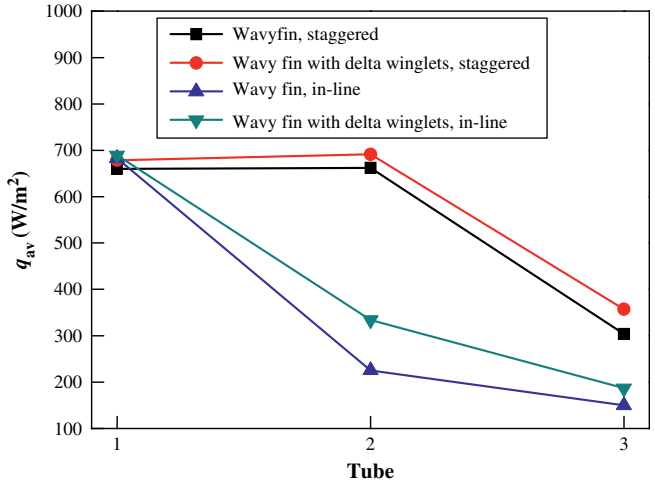

Fig. 13. Variation of area-averaged tube surface heat flux in staggered and in-line arrangements.

Table 2
Summary of Colbum and friction factors for staggered and in-line arrangements at $Re_{D_c} = 3000$.

	In-line		Staggered	
	Wavy fin (baseline)	Wavy fin with delta winglets	Wavy fin (baseline)	Wavy fin with delta winglets
j	0.01116	0.01288	0.01392	0.01575
j/j_0	1	1.154	1	1.131
f	0.04748	0.05248	0.05499	0.05884
f/f_0	1	1.105	1	1.070
j/f	0.235	0.245	0.253	0.268
$(j/j_0)/(f/f_0)$	1	1.044	1	1.057
$JF=(j/j_0)/(f/f_0)^{1/3}$	1	1.166	1	1.106

enhancement is usually accompanied by additional pressure loss and pumping power increase. In order to evaluate the overall performance of the wavy fin-and-tube heat exchanger with delta winglets, the comparison in area goodness factor defined as j/f is summarized in Table 2. In the staggered and in-line arrays, the area goodness factors of the wavy fin with delta winglets are larger than that of the respective baseline case. At the same time, the JF-factor defined as $JF=(j/j_0)/(f/f_0)^{1/3}$ is also summarized in Table 2 as another way to compare the performance of the wavy fin with delta winglets with that of the baseline fin for the same pumping power. The JF-factors of the wavy fin with delta winglets are 1.166 and 1.106 for in-line and staggered arrays, respectively. These results show that the delta winglet cause considerable augmentation of heat transfer capacity for the wavy fin with modest pressure drop penalty and improve the overall performance of the wavy fin-and-tube heat exchanger.

6. Conclusions

The paper presents a three-dimensional numerical simulation on the air-side performance of a wavy fin-and-tube heat exchanger with delta winglets. The effects of the delta winglet on the flow structure and heat transfer performance of the wavy fin channel are investigated, and the comparison of the fluid flow and heat transfer characteristics between staggered and in-line arrangements is explored. The major findings are summarized as follows.

(1) The delta winglet generates a downstream main vortex and a corner vortex, the main vortex is formed by flow separation at the leading edge of the delta winglet, the corner vortex having the horseshoe vortex-like characteristic feature is generated at the junction of the front face of the winglet and

the fin surface. The intensity of the corner vortex is weaker than that of the main vortex.

(2) For the in-line array, the longitudinal vortices generated by the delta winglet develop downstream for a long distance, the increase of the cross-section circulation downstream of delta winglet lasts until the position corresponding to the center of the downstream tube. While for the staggered array, due to the blockage of the downstream tube and the change of the main-flow direction, the longitudinal vortices are disrupted at the downstream wavy trough only developing a short distance along the main-flow direction.

(3) The longitudinal vortices not only decrease the wake zone size behind the tube, but also increase the flow velocity in the wake region. The maximum increases of local heat transfer coefficient of the wavy fin with delta winglets are 80% and 95% compared with the wavy fin without delta winglets in staggered and in-line arrangements, respectively. The longitudinal vortices obviously improve the heat transfer of the fin surface in the tube wake region.

(4) For the in-line array, the longitudinal vortices enhance the heat transfer not only on the fin surface of the wake region but also on the tube surface downstream of the delta winglet. The heat flux of the first, second and third row tube surface in the wavy fin with delta winglets is increased by 1%, 48% and 25%, respectively. However, for the staggered array, only the heat flux augment of the third row tube by the longitudinal vortices is obvious, the heat flux of the first, second and third row tube surfaces is increased by 3%, 4% and 18%, respectively.

(5) The delta winglet enhances the heat transfer of the fin channel, and increases the pressure drop, but the increase of the heat transfer is larger than that of the pressure drop. For the in-line array, compared with the wavy fin, the j and f factors of the wavy fin with delta winglets are increased by 15.4% and 10.5%, respectively. For the staggered array, the j and f factors are increased by 13.1% and 7.0%, respectively.

(6) For both staggered and in-line arrangements, the longitudinal vortices generated by the delta winglet significantly enhance the heat transfer of the wavy fin-and-tube heat exchanger, and improve the overall performance of the heat exchanger.

Acknowledgements

The present work is supported by the Key Project of National Natural Science Foundation of China (No. 50736005), and National Basic Research Program of China (973 Program) (2007CB206902).

References

[1] A.M. Jacobi, R.K. Shah, Heat transfer surface enhancement through the use of longitudinal vortices: a review of recent progress, Exp. Therm. Fluid Sci. 11 (1995) 295–309.
[2] G.B. Schubauer, W.G. Spangenberg, Forced mixing in boundary layers, J. Fluid Mech. 8 (1960) 10–31.
[3] T.R. Johnson, P.N. Joubert, The influence of vortex generators on drag and heat transfer from a circular cylinder normal to an airstream, ASME J. Heat Transf. 91 (1969) 91–99.
[4] M.C. Gentry, A.M. Jacobi, Heat transfer enhancement by delta-wing vortex generators on a flat plate: vortex interactions with the boundary layer, Exp. Therm. Fluid Sci. 14 (1997) 231–242.
[5] M.C. Gentry, A.M. Jacobi, Heat transfer enhancement by delta-wing-generated tip vortices in flat-plate and developing channel flows, ASME J. Heat Transf. 124 (2002) 1158–1168.
[6] G. Biswas, K. Torii, D. Fujii, K. Nishino, Numerical and experimental determination of flow structure and heat transfer effects of longitudinal vortices in a channel flow, Int. J. Heat Mass Transf. 39 (1996) 3441–3451.
[7] C.C. Wang, J. Lo, Y.T. Lin, C.S. Wei, Flow visualization of annular and delta winglet vortex generators in fin-and-tube heat exchanger application, Int. J. Heat Mass Transf. 45 (2002) 3803–3815.
[8] Y. Chen, M. Fiebig, N.K. Mitra, Heat transfer enhancement of a finned oval tube with punched longitudinal vortex generators in-line, Int. J. Heat Mass Trans. 41 (1998) 4151–4166.
[9] Y. Chen, M. Fiebig, N.K. Mitra, Heat transfer enhancement of finned oval tubes with staggered punched longitudinal vortex generators, Int. J. Heat Mass Transf. 43 (2000) 417–435.
[10] S. Tiwari, D. Maurya, G. Biswas, V. Eswaran, Heat transfer enhancement in cross-flow heat exchangers using oval tubes and multiple delta winglets, Int. J. Heat Mass Transf. 46 (2003) 2841–2856.
[11] J.E. O'Brien, M.S. Sohal, P.C. Wallstedt, Local heat transfer and pressure drop for finned-tube heat exchangers using oval tubes and vortex generators, ASME J. Heat Transf. 126 (2004) 826–835.
[12] J.E. O'Brien, M.S. Sohal, Heat transfer enhancement for finned-tube heat exchangers with winglets, ASME J. Heat Transf. 127 (2005) 171–178.
[13] J.S. Leu, Y.H. Wu, J.Y. Jang, Heat transfer and fluid flow analysis in plate-fin and tube heat exchangers with a pair of block shape vortex generators, Int. J. Heat Mass Transf. 47 (2004) 4327–4338.
[14] S.M. Pesteei, P.M.V. Subbarao, R.S. Agarwal, Experimental study of the effect of winglet location on heat transfer enhancement and pressure drop in fin-tube heat transfer, Appl. Therm. Eng. 25 (2005) 1684–1696.
[15] G. Biswas, N.K. Mitra, M. Fiebig, Heat transfer enhancement in fin-tube heat exchangers by winglet type vortex generators, Int. J. Heat Mass Transf. 37 (1994) 283–291.
[16] K. Torii, K.M. Kwak, K. Nishino, Heat transfer enhancement accompanying pressure-loss reduction with winglet-type vortex generators for fin-tube heat exchangers, Int. J. Heat Mass Transf. 45 (2002) 3795–3801.
[17] K.M. Kwak, K. Torii, K. Nishino, Simultaneous heat transfer enhancement and pressure loss reduction for finned-tube bundles with the first or two transverse rows of built-in winglets, Exp. Therm. Fluid Sci. 29 (2005) 625–632.
[18] C.B. Allison, B.B. Dally, Effect of a delta-winglet vortex pair on the performance of a tube-fin heat exchanger, Int. J. Heat Mass Transf. 50 (2007) 5065–5072.
[19] L.B. Wang, F. Ke, S.D. Gao, Y.G. Mei, Local and average characteristics of heat/mass transfer over flat tube bank fin with four vortex generators per tube, ASME J. Heat Transf. 124 (2002) 546–552.
[20] M.L. Smotrys, H. Ge, A.M. Jacobi, J.C. Dutton, Flow and heat transfer behavior for a vortex-enhanced interrupted fin, ASME J. Heat Transf. 125 (2003) 788–794.
[21] A. Joardar, A.M. Jacobi, Impact of leading edge delta-wing vortex generators on the thermal performance of a flat tube, louvered-fin compact heat exchanger, Int. J. Heat Mass Transf. 48 (2005) 1480–1493.
[22] P.A. Sanders, K.A. Thole, Effects of winglets to augment tube wall heat transfer in louvered fin heat exchangers, Int. J. Heat Mass Transf. 49 (2006) 4058–4069.
[23] F. Dupont, C. Gabillet, P. Bot, Experimental study of the flow in a compact heat exchanger channel with embossed-type vortex generators, ASME J. Heat Transf. 125 (2003) 701–709.
[24] Y.B. Tao, Y.L. He, J. Huang, Z.G. Wu, W.Q. Tao, Three-dimensional numerical study of wavy fin-and-tube heat exchangers and field synergy principle analysis, Int. J. Heat Mass Transf. 50 (2007) 1163–1175.
[25] Y.B. Tao, Y.L. He, Z.G. Wu, W.Q. Tao, Three-dimensional numerical study and field synergy principle analysis of wavy fin heat exchangers with elliptic tubes, Int. J. Heat Fluid Flow 28 (2007) 1531–1544.
[26] Y.B. Tao, Y.L. He, J. Huang, Z.G. Wu, W.Q. Tao, Numerical study of local heat transfer coefficient and fin efficiency of wavy fin-and-tube heat exchangers, Int. J. Therm. Sci. 46 (2007) 768–778.
[27] W.Q. Tao, Numerical Heat Transfer, second ed. Xi'an Jiaotong University Press, Xi'an, China, 2001.
[28] FLUENT Incorporated, FLUENT 6.2 User's Guide, Fluent Incorporated Lebanon, NH, USA, 2004.
[29] T.E. Schmidt, Heat transfer calculations for extended surfaces, Refrig. Eng. (April 1949) 351–357.
[30] R.C. Xin, H.Z. Li, H.J. Kang, W. Li, W.Q. Tao, An experimental investigation on heat transfer and pressure drop characteristics of triangular wavy fin-and-tube heat exchanger surfaces, J. Xi'an Jiaotong Univ. 28 (2) (1994) 77–83.
[31] W. Xue, J.C. Min, Numerical predictions of fluid flow and heat transfer in corrugated channels, in: Proceedings of the 3rd Int. Symposium on Heat Transfer and Energy Conservation, Guangzhou, China, January 12–15, vol. 1, 2004, pp. 714–721.
[32] Y.L. He, W.Q. Tao, F.Q. Song, W. Zhang, Three-dimensional numerical study of heat transfer characteristics of plain plate fin-and-tube heat exchangers from view point of field synergy principle, Int. J. Heat Fluid Flow 26 (2005) 459–473.
[33] R.R. Méndez, M. Sen, K.T. Yang, R.L. McClain, Enhancement of heat transfer in an inviscid-flow thermal boundary layer due to a Rankine vortex, Int. J. Heat Mass Transf. 41 (1998) 3829–3840.